Kinetics of motility-induced phase separation and swim pressure

Adam Patch,[1,*] David Yllanes,[1,2] and M. Cristina Marchetti[1]
[1]*Department of Physics and Soft Matter Program, Syracuse University, Syracuse, New York 13244, USA*
[2]*Instituto de Biocomputación y Física de Sistemas Complejos (BIFI), 50009 Zaragoza, Spain*
(Received 7 October 2016; published 5 January 2017)

Active Brownian particles (ABPs) represent a minimal model of active matter consisting of self-propelled spheres with purely repulsive interactions and rotational noise. Here we examine the pressure of ABPs in two dimensions in both closed boxes and systems with periodic boundary conditions and show that its nonmonotonic behavior with density is a general property of ABPs and is not the result of finite-size effects. We correlate the time evolution of the mean pressure towards its steady-state value with the kinetics of motility-induced phase separation. For parameter values corresponding to phase-separated steady states, we identify two dynamical regimes. The pressure grows monotonically in time during the initial regime of rapid cluster formation, overshooting its steady-state value and then quickly relaxing to it, and remains constant during the subsequent slower period of cluster coalescence and coarsening. The overshoot is a distinctive feature of active systems.

DOI: 10.1103/PhysRevE.95.012601

I. INTRODUCTION

Over the past decade, there has been growing interest in the physics of active matter, defined as collections of self-driven particles that exhibit rich emergent behavior [1]. Realizations abound in the living world, from bird flocks [2–4] to epithelial cell monolayers [5,6], and in engineered systems, such as self-catalytic colloids [7,8] and microswimmers [9]. The distinctive property of active systems is that the particles are independently driven out of equilibrium and time reversal symmetry is broken locally, rather than globally as in systems driven out of equilibrium by external fields or boundary forces.

Progress has recently been made in formulating the nonequilibrium statistical mechanics of active matter using a minimal model of active Brownian particles (ABPs) consisting of purely repulsive self-propelled spherical colloids with overdamped dynamics [10]. Perhaps the most remarkable property of this simple system is that it spontaneously phase separates into a dense liquid phase and a gas phase in the absence of any attractive interactions [10–15]. This phenomenon arises from the persistent dynamics of self-propelled particles when the time for particles to reorient after a collision exceeds the mean-free time between collisions, hence the name motility-induced phase separation (MIPS). Additionally, in a sort of reverse MIPS, confined ABPs spontaneously accumulate at the walls of the container [16–18], a behavior which is at odds with fundamental properties of gases and fluids in thermal equilibrium. These findings have raised a lot of interest in understanding whether active matter can be characterized in terms of equilibrium-like properties, such as effective temperature and pressure. A broad class of active particles can exert persistent forces on the walls of a container. These forces have been quantified recently in terms of a new contribution to the pressure, dubbed swim pressure, that measures the flux of propulsive forces across a unit bulk plane of material [17,19]. Remarkably, it has been shown that in generic active systems the mechanical force exerted on the walls of the container depends on the detail of particle-wall interactions, making it impossible to define the pressure of an active fluid as a state function [20].

This result, however, does not apply to the special case of spherical ABPs. For this minimal model it has been shown that the pressure is indeed a state function that characterizes the bulk material properties of this simple active fluid [20,21]. On the other hand, the behavior of pressure of spherical ABPs is unusual, in that simulations have reported a nonmonotonic behavior of pressure versus density, arising from the suppression of motility (and therefore of swim pressure) associated with particle caging at the onset of phase separation [17,22]. Experimental measurements of pressure of active colloids have similarly shown a strong suppression of pressure at intermediate density [8]. In spite of extensive work, open questions remain concerning the quantitative role of finite-size effects in active systems and the origin and robustness of the nonmonotonic behavior of pressure.

In this paper we use molecular dynamics simulations to investigate the pressure of spherical ABPs with soft repulsive forces and correlate its nonmonotonic behavior with density with the kinetics of cluster size growth in phase-separating systems. By examining both systems bounded by confining walls and ones with periodic boundary conditions, we show that finite-size effects are consistent in both cases with the behavior expected for a rarefied thermal gas. The pressure calculated in confined systems is strongly suppressed by the presence of boundaries if the persistence length of the particles dynamics is comparable to the linear size of the container, with a linear dependence on system size and a behavior that resembles that of a rarified Knudsen gas. With periodic boundary conditions the convergence to the large system size limit is exponential, again as expected in a thermal system.

The nonmonotonic behavior of pressure as a function of density for repulsive ABPs with large persistence lengths was first reported in simulations of systems in closed boxes [17] and has been seen in sedimentation experiments of active colloids [8]. More recently it was confirmed in numerical studies of hard active particles with periodic boundary conditions in three dimensions [22]. Our work provides a systematic study of finite-size effects in both bounded and periodic systems and shows that the nonmonotonicity is not a finite-size effect, but a bulk properties of ABPs. It arises because in phase-separated systems the aggregate effectively provides a bounding wall

*Corresponding author: apatch@syr.edu

for the active gas, which suppresses the swim pressure. Additionally, by considering soft repulsive disks, we complement previous work on hard particles and show that this effect does not depend on the details of the interparticle interaction. Finally, we examine the kinetics of coarsening and establish a strong correlation between the aggregation dynamics and the relaxation of the pressure towards its steady-state value. We identify two dynamical regimes that control the relaxation of a disordered initial state towards the nonequilibrium steady state of the system. For system parameters that produce a homogeneous steady state, pressure grows monotonically in time to its steady-state value, which it reaches on a time scale controlled by the persistence time of the self-propelled dynamics. In contrast, for parameters that produce a phase-separated steady state, the time evolution of the pressure is not monotonic, and there are two dynamical regimes. Initially, small clusters form and break up rapidly, and the pressure quickly builds and overshoots its asymptotic value. Eventually the dynamics crosses over to a coarsening regime with a slower cluster growth, and the pressure relaxes to its steady-state value.

The rest of the paper is organized as follows. Section II describes the ABP model and provides details of our simulations. Section III examines the swim pressure and its behavior at low and high density. It also discusses the relevance of finite-size effects. Section IV examines correlations between the pressure relaxation and the kinetics of MIPS of swim pressure. Finally, we close in Sec. V with some concluding remarks.

II. ACTIVE BROWNIAN PARTICLES MODEL

We consider a well-established minimal model of monodispersed ABPs in two dimensions [10], consisting of N self-propelled disks of radius a in a square box of area L^2. Each particle is identified by the position $\boldsymbol{r}_i$ of its center and a unit vector $\hat{\boldsymbol{e}}_i = (\cos\theta_i, \sin\theta_i)$ that defines the axis of self-propulsion. Assuming the medium provides only friction, the dynamics is governed by Langevin equations, given by

$$\dot{\boldsymbol{r}}_i = v_0\hat{\boldsymbol{e}}_i + \mu\sum_{j\neq i}\boldsymbol{F}_{ij}, \tag{1}$$

$$\dot{\theta}_i = \eta_i(t), \tag{2}$$

where v_0 is the bare self-propulsion speed, directed along $\hat{\boldsymbol{e}}_i$, and $\eta_i(t)$ a Gaussian random torque with zero mean and variance $\langle\eta_i(t)\eta_j(t')\rangle = 2D_r\delta_{ij}\delta(t-t')$, with D_r the rate of rotational diffusion. The pair forces $\boldsymbol{F}_{ij}$ are purely repulsive and harmonic, with $\boldsymbol{F}_{ij} = k(2a - r_{ij})\hat{\boldsymbol{r}}_{ij}$ for $r < 2a$ and $F_{ij} = 0$ otherwise, where $\boldsymbol{r}_{ij} = \boldsymbol{r}_i - \boldsymbol{r}_j$ is the interparticle separation and $\hat{\boldsymbol{r}}_{ij} = \boldsymbol{r}_{ij}/|\boldsymbol{r}_{ij}|$. Finally, μ is the mobility. We neglect here noise in the translational dynamics, which is less important than the orientational one in both synthetic active colloids and swimming bacteria [15]. The nonequilibrium nature of this minimal active model is provided entirely by the propulsive force $\boldsymbol{F}_i^s = (v_0/\mu)\hat{\boldsymbol{e}}_i$. After integrating out the angular dynamics, $\boldsymbol{F}_i^s$ represents a non-Markovian stochastic force correlated over the persistence time $\tau_r = D_r^{-1}$. Since the finite correlation time of the noisy propulsive force is not matched by similar correlations in the friction coefficient μ^{-1}, which is constant, the system does not obey the equilibrium fluctuation-dissipation theorem embodied by the Stokes-Einstein relation.

The persistence time τ_r controls the crossover from ballistic to diffusive regime in the single-particle dynamics. For $t \gg \tau_r$ the dynamics of noninteracting ABPs is diffusive, with diffusion coefficient $D_s = v_0^2\tau_r/2$. The single-particle dynamics can also be characterized by the persistence length, $\ell_p = \frac{v_0}{D_r}$, and the rotational Péclet number, $Pe_r = \ell_p/a$, used in much of the literature [13,15].

Our simulations employ a conventional Brownian dynamics algorithm [23]. We take the interaction time scale, $\tau_D = (\mu k)^{-1}$, as the unit time ($\mu = k = 1$) and the particle radius a as the unit of length ($a = 1$). To prevent particles from passing through each other, we set $v_0 = (a\mu k)/100$. We choose a time step sufficiently small to handle many-body interactions at high density, $\delta t \ll \tau_D$.

As discussed in the introduction, purely repulsive ABPs exhibit macroscopic phase separation, or MIPS, where the dense phase grows to the size of the system and nearly free particles in the gas phase try to explore lengths of order ℓ_p. For this reason, ABPs are subject to strong finite-size effects that we quantify here by considering simulation boxes of linear size $L = 50, 100, 200, 400$, both in a closed box geometry and with periodic boundary conditions. We tune the packing fraction $\phi = N\frac{\pi a^2}{L^2}$ that sets the total number of particles, N, with $N \sim 10^5$ for $L = 400$. A schematic representation of the region of the phase diagram explored in the present work is shown in Fig. 1, where the color represents the variance of the local density. Phase-separated systems are plotted with circles.

All simulations have been run for a time t_f of 10^6 time units or longer, which in all cases is several orders of magnitude longer than the time scale of the particles' rotational diffusion: $t_f \gtrsim 500D_r^{-1}$. To examine the time evolution of

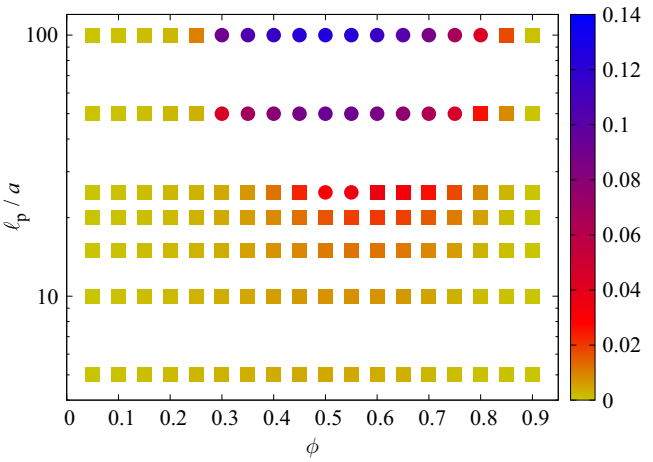

FIG. 1. Phase diagram of ABPs for a system of size $L = 200$ in the plane of packing fraction ϕ and persistence length ℓ_p. The phase diagram is constructed by examining the probability distribution $P(\phi_W)$ of the local densities, computed by dividing the system in N_W windows of size 20×20 and calculating the packing fraction ϕ_W in each window. The heat map shows the values of the variance of this distribution, defined as $\sigma_W^2 = \frac{1}{N_W}\sum_{i=1}^{N_W}\langle(\phi_W - \phi)^2\rangle$. In phase-separated states, the probability distribution of ϕ_W is bimodal (see, e.g., Ref. [13]) and σ_W^2 is large. We show with circles those values of the parameters that result in a $P(\phi_W)$ with two peaks (gas density and aggregate density).

our observables, we average the relevant physical quantities over exponentially increasing time windows. In particular, we use the so-called $\log_2$-binning procedure by following the evolution of averages in time intervals $I_n = (2^{-(n+1)}t_f, 2^{-n}t_f]$. The error bars are estimated from the fluctuations between several independent runs with a jackknife procedure (see, e.g., Ref. [24]). We have 500 runs for $\phi = 0.01$ and 10–20 runs for larger values of ϕ.

We also use this time binning procedure to assess convergence to the steady state. We consider the simulation to have reached a steady state if the averages in at least the first three I_n are compatible with each other within errors. If this condition is not met, we double the simulation time. In particular for parameter values where the system phase separates, simulations have been run for 10^7 time units.

Finally, we shall denote our estimate of the steady-state ensemble average of an observable O by $\langle O\rangle$, which we compute by taking the value for the I_0 time interval (i.e., the last half of the simulations).

III. SWIM PRESSURE

There has recently been a lot of interest in characterizing the pressure of active systems. Pressure can be defined in terms of the forces transmitted across a unit bulk plane of material. In an active fluid there is a unique contribution to pressure that measures the flux of propulsive forces across a bulk plane of material [17,21,25]. This contribution, dubbed swim pressure in recent literature [26], can be expressed via a virial-type formula as [15,17,19]

$$p_s = \frac{1}{dL^2}\sum_i \boldsymbol{F}_i^s \cdot \boldsymbol{R}_i, \tag{3}$$

with d the spatial dimension (here $d = 2$). In a closed box $\boldsymbol{R}_i = \boldsymbol{r}_i$, but with periodic boundary conditions $\boldsymbol{R}_i$ is the position of the particle in an infinite system, accounting for winding numbers as the particle crosses the periodic boundary [27,28]. The virial expression estimates the swim pressure as the propulsive force carried over a distance of the order of the persistence length, in analogy to the kinetic pressure of an ideal gas or the radiation pressure of a photon gas. Note, however, that in spite of the one-body expression given in Eq. (3), the swim pressure depends on interactions that lead to suppression of the persistence length. In addition to the swim pressure, there is also the contribution describing the direct transmission of interaction forces across the bulk plane. For pairwise forces $\boldsymbol{F}_{ij}$, as relevant to our collection of ABPs, this can be calculated from the familiar virial expression

$$p_D = \frac{1}{dL^2}\sum_{i,j} \boldsymbol{F}_{ij} \cdot \boldsymbol{r}_{ij}. \tag{4}$$

Recent work has shown that for the minimal model of spherical ABPs considered here the total pressure $p = p_s + p_D$ defined from Eqs. (3) and (4) coincides with the force per unit area on the walls of a container [17] and represents a state function of the active fluid [20], independent of the properties of the walls.

In the remainder of this section we examine the importance of finite-size effects in the calculation of the pressure of active systems and demonstrate that the predicted [17] and observed [8] nonmonotonicity of pressure versus density is an intrinsic property of these nonequilibrium fluids, not a finite-size effect.

A. Pressure of a dilute active gas

For a dilute gas of ABPs, the dominant contribution to the pressure comes from the swim pressure p_s. Neglecting interactions, and in the large-size limit, Eq. (3) can be calculated exactly, with the result [17,29]

$$p(t) = p_0(1 - e^{-D_r t}), \quad p_0 = \rho\frac{v_0^2}{2\mu D_r}, \tag{5}$$

where $\rho = N/L^2 = \phi/(\pi a^2)$ is the number density. The pressure p_0 of an active ideal gas can be naturally interpreted in terms of an active temperature, with $p_0 = \rho k_B T_a$, and $T_a = v_0^2/(2\mu k_B D_r)$. This active temperature also coincides with the one set by the ratio of translational diffusion $D_s = v_0^2\tau_r/2$ to the friction coefficient μ^{-1}, as required for thermal Brownian particles satisfying the Stokes-Einstein relation. Indeed, the stochastic propulsive force becomes δ-correlated in time in the limit $\tau_r \to 0$, with $k_B T_a = $ constant [10]. In other words, noninteracting ABPs behave like thermal colloids at temperature T_a in the limit of vanishing persistence time, τ_r. Here we consider the pressure of active particles for finite values of the persistence time, away from this Brownian limit.

The time evolution of p_s of a dilute active gas ($\phi = 0.01$) is shown in Fig. 2 for a system in a box of linear size $L = 200$ with periodic boundary conditions (a) and one enclosed by bounding walls (b), for various values of the persistence length, ℓ_p. Flat repulsive walls are implemented using the same harmonic forces that describe interparticle interactions.

For periodic boundary conditions, Eq. (5) provides an excellent fit to the calculated pressure over the entire time range and for all ℓ_p considered. In confined systems, however, a second time scale comes into play, the time $\tau_L = L/v_0$ it takes an ABP to travel the size of the box. The finite-size corrections to pressure are negligible only when $\tau_L \gg \tau_r$, or equivalently $L \gg \ell_p$ (here with $L = 200$ this only holds for the smallest $\ell_p = 5$). In all other cases the presence of confining walls strongly suppresses the asymptotic long-time value of the pressure as compared to the value p_0 given by Eq. (5). To quantify the finite-size corrections, the insets of Fig. 2 show the ratio $\langle p\rangle/p_0$ of the calculated steady-state pressure to the ideal active gas pressure as a function of ℓ_p for various system sizes L. With periodic boundary conditions (a), the finite-size corrections are essentially independent of ℓ_p and converge very quickly to p_0 with increasing system size; in fact, for $L = 200$ $\langle p(\ell_p)\rangle/p_0$ is indistinguishable from 1 with our errors.

In the case of the closed box the finite-size effects are much more pronounced and depend strongly on ℓ_p, as shown in the inset of Fig. 2(b). Our $\langle p\rangle/p_0$ for different L can be nearly collapsed when plotted versus ℓ_p/L. In fact, for $\ell_p/L \lesssim 0.1$, the behavior can be fitted by a linear form, $\langle p\rangle/p_0 \simeq 1 - A\ell_p/L$. This functional dependence supports the idea that the box boundary has a simple surface effect on the pressure for $\ell_p/L \ll 1$. At higher persistence lengths, collective effects, such as clustering of particles at the corners of the box, yield further deviations from the linear behavior.

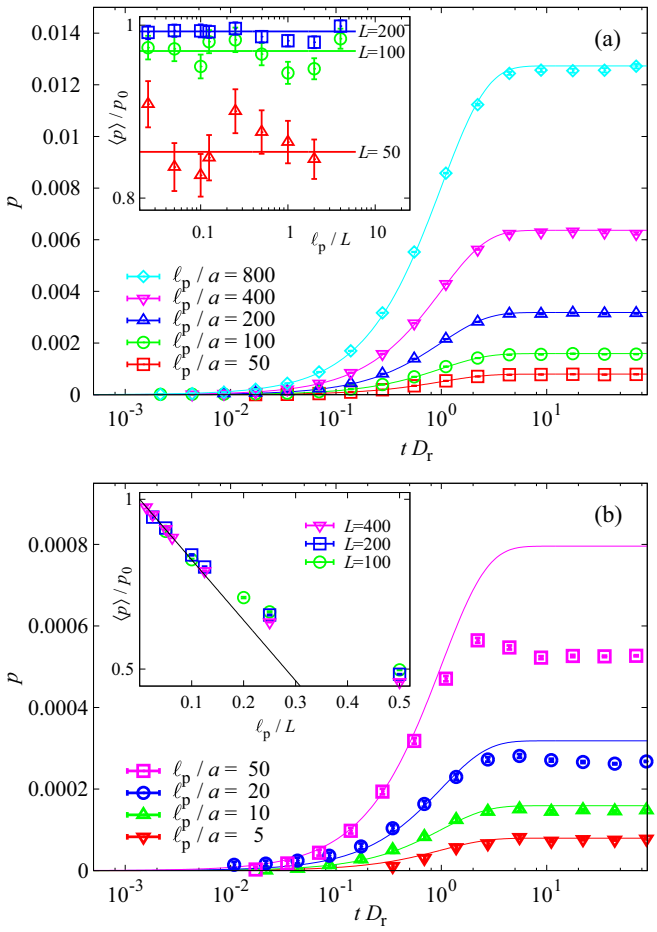

FIG. 2. Time evolution of the pressure of a dilute gas ($\phi = 0.01$) of ABPs for various values of the persistence length for periodic (a) and closed (b) square boxes of linear size $L = 200$. At this density the pressure is determined entirely by the swim pressure. The solid lines show the large-L ideal gas prediction of Eq. (5), which matches the numerical results for periodic boundary conditions even at very large ℓ_p. For closed systems the pressure is significantly suppressed by accumulation of particles at the walls as soon as ℓ_p becomes comparable to L. The insets show our estimate for the steady-state pressure $\langle p \rangle$ in the dilute limit divided by the ideal gas steady-state value $p_0 = \rho v_0 \ell_p / 2\mu$ as a function of persistence length for a various systems sizes L. For periodic boundary conditions [(a), inset] the system is self-averaging and $\langle p \rangle^{(L)} \approx p_0$ within errors for $L = 200$. For the closed box [(b), inset], there are strong finite-size effects due to the walls. We show that $\langle p \rangle / p_0$ versus ℓ_p / L can be fit to $1 - A\ell_p/L$ for $\ell_p/L \leqslant 0.1$ (black line) with a result of $A = 1.78(3)$, $\chi^2 = 7.16$ for 6 degrees of freedom (d.o.f.).

In summary, we find that at low density the swim pressure is clearly suppressed in systems that restrict the mean-free path below ℓ_p, so that the dynamics remains ballistic at all times. When particles are confined, there are strong boundary effects reminiscent of those seen in a Knudsen gas, where the density is so low that the mean-free path from interparticle collisions exceeds the box size. Specifically, the convergence to the large-L limit is exponential for the periodic box and linear for the closed box. This is precisely the type of the finite-size effects one expects in a thermal system whose free energy would have bulk and surface contributions, with the former the only relevant one in periodic systems at large L.

B. Pressure at finite density

At finite density, both the swim contribution and the direct contribution from interactions are appreciable. The direct contribution from interactions, $p_D(\phi)$, grows monotonically with density as in passive systems and depends only weakly on self propulsion [17]. In contrast the swim pressure is nonmonotonic in density and strongly suppressed at intermediate density due to the decrease of particle motility. This leads to an overall nonconvex density dependence of the total pressure $\langle p(\phi) \rangle$, which has been seen in simulations [17,20,22] and experiments [8]. For larger ℓ_p simulations show a nonmonotonic $\langle p(\phi) \rangle$.

When the system phase separates, the macroscopic aggregate effectively provides a bounding wall to the gas phase, leading to strong finite-size effects in the swim pressure even in systems with periodic boundary conditions. This is shown in Fig. 3. Here the bottom frame ($\ell_p/a = 50$) shows a system which undergoes phase separation for intermediate densities, while in the top frame ($\ell_p/a = 25$) the phase separation is still incipient (recall Fig. 1). We note that in the former case we need box sizes of $L \geqslant 200$ to achieve convergence [30]. All

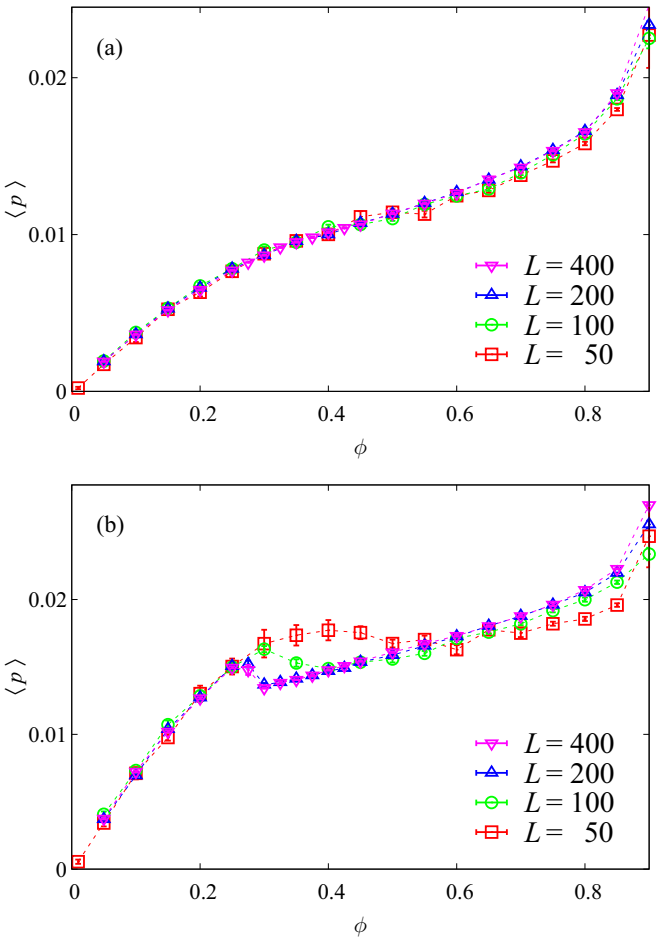

FIG. 3. Pressure as a function of packing fraction for $\ell_p/a = 25$ (a) and $\ell_p/a = 50$ (b) for a system with periodic boundary conditions. The box size must be several times larger than ℓ_p to obtain results representative of the large-L limit.

the results reported in the remainder of the paper are for box sizes $L = 200,400$, and are free of finite-size effects within our error bars.

For sufficiently large values of ℓ_p the pressure of the active fluid is nonmonotonic with density. This behavior, shown in Fig. 3(b), is not a finite-size effect and is associated with the strong suppression of the swim pressure arising from motility-induced aggregation. Reference [20] showed that the suppression of p_s can be captured by a simple expression, given by

$$p_s = \rho \frac{v_0 v(\rho)}{2\mu D_r}, \tag{6}$$

with $v(\rho) = v_0 + \mu \langle \hat{\boldsymbol{e}}_i \cdot \sum_{j \neq i} \boldsymbol{F}_{ij} \rangle$ the effective velocity of a particle along its direction of self-propulsion. To leading order in the density, this has a linear decay $v(\rho) = v_0(1 - \rho/\rho_*)$, where $\rho_* \equiv \rho_*(\ell_p)$ provides a cutoff, above which $v(\rho)$ goes to zero. Inserting this form of $v(\rho)$ into Eq. (6) yields a quadratic form for the swim pressure, $p_s = k_B T_a \rho(1 - \rho/\rho_*)$ [20].

As we can see in Fig. 4(a), this ansatz works well only for moderate ℓ_p ($\ell_p/a \lesssim 25$ with our parameters). For large ℓ_p, i.e., for systems exhibiting phase separation (see Fig. 1), the swim pressure displays a much stronger dependence on density and drops abruptly at the onset of phase separation. Phase-separating systems always evolve to contain a single large dense region,

The relation between pressure and particle aggregation is shown in Fig. 4. The bottom frame displays the total number of particles N_c that belong to clusters above a certain threshold size (we use a cutoff of 100) [31]. The sharp drop in pressure shown in Fig. 4(a) at large values of ℓ_p corresponds to a jump in the value of N_c, signaling the onset of phase separation. A similar result has been obtained for hard repulsive spheres in $d = 3$ [22].

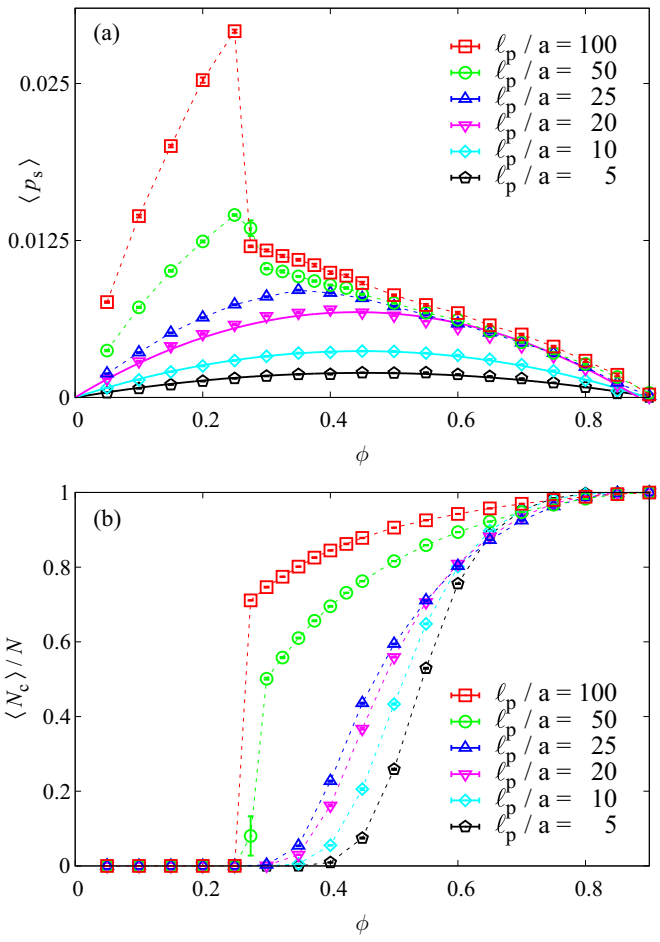

FIG. 4. Swim pressure $\langle p_s \rangle$ (a) and cluster fraction $\langle N_c \rangle / N$ (b) versus packing fraction ϕ for several values of ℓ_p (we use $L = 200$ for $\ell_p/a \leqslant 25$ and $L = 400$ for $\ell_p/a = 50,100$). In (a), solid lines show fits to $\langle p_s \rangle = p_0(\phi)(1 - \phi/\phi_0)$, where ϕ_0 is the only adjustable parameter (see Ref. [15]). This quadratic behavior breaks down for higher ℓ_p. In both frames, dashed lines provide a guide for the eye.

IV. KINETICS OF MOTILITY-INDUCED PHASE SEPARATION

The time evolution of the pressure from a random initial condition towards the final steady state reveals a nonmonotonic dynamics directly related to the kinetics of MIPS. This is displayed in Fig. 5. For parameter values corresponding to homogeneous steady states, the pressure evolves monotonically in time, reaching its steady-state value in a time of the order of the persistence time, τ_r. For parameter values corresponding to phase-separated steady states, however, the convergence to the steady state is delayed by cluster nucleation and aggregation, which operate on a density-dependent time scale much longer than rotational diffusion. This results in the pressure temporarily overshooting its steady-state value, as shown in Fig. 5. The total time required for the pressure to reach steady state depends on density and, not surprisingly, is longest for the lowest densities that exhibit phase separation. The growth of the dense phase is associated with the formation

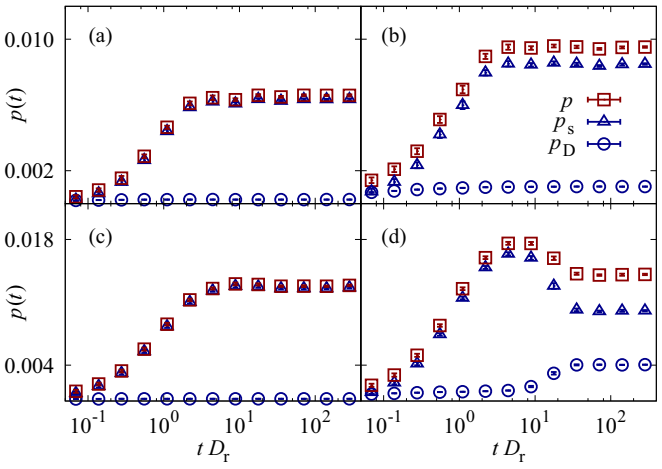

FIG. 5. Time evolution of the total pressure p (red squares), swim pressure p_s (blue triangles), and direct pressure p_D (blue circles) for $\ell_p/a = 25$ and $\phi = 0.2$ (a), $\ell_p/a = 25$ and $\phi = 0.35$ (b), $\ell_p/a = 50$ and $\phi = 0.2$ (c), and $\ell_p/a = 50$ and $\phi = 0.35$ (d). Systems that remain homogeneous reach steady state on the time scale of $\tau_r = D_r^{-1}$ while phase-separating systems (in this case $\phi = 0.35$, $\ell_p = 50$, recall Fig. 1) take orders of magnitude longer. Swim and total pressures grow nonmontonically, first reaching a maximum value on the time scale of τ_r, then falling to a lower steady-state value on a density-dependent time scale related to the increased variance of nucleation times at lower densities.

of clusters of jammed particles. If the reorientation time τ_r required for particles to turn and escape from the cluster is longer than the mean-free time between collisions, more particles will accumulate and the cluster will grow. This process continues as long as the rate for escaping from the cluster (D_r), is slower than the rate at which particles absorb at the boundary, which is controlled by the collision rate. Systems with lower densities take a longer time to reach the final state due to lower nucleation and adsorption cross sections. This is in agreement with recent work examining the kinetics of MIPS in terms of classical nucleation theory [32].

By comparing the evolution of pressure and of density correlations in our largest phase-separating systems ($L = 400$), we can identify two distinct dynamical regimes. Once the pressure reaches its steady-state value, clusters begin to coarsen at a slower rate, corresponding to previous observations [33,34].

By the time pressure equilibrates, multiple clusters have formed, and there is an average zero net flux between phases, shown in Fig. 6, where we additionally quantify the number of particles in the largest cluster N_1 alongside all clustered particles N_c. At this stage, the dense aggregates move very slowly, having caged the motility of most aggregated particles, only allowing those at the boundary to deadsorb, while large clusters coalesce into one another until system-spanning phase separation occurs. We find a division in time regimes of growth for $N_c(t)$ and $N_1(t)$ and show snapshots of this process in Fig. 6. The largest cluster continues to grow long after the cluster fraction saturates, which corresponds with pressure reaching its steady state.

In particular, for the data shown in Fig. 6, we have fit the number of particles in the largest cluster to

$$N_1(t) \sim t^{\gamma}. \tag{7}$$

In the first time regime (up to and including point B in the figure, that is, for $t D_r < 20$) this fit gives $\gamma_1 = 1.3(2), \chi^2/\text{d.o.f.} = 0.12/1$. In the coarsening regime, for $t D_r > 20$, we obtain $\gamma_2 = 0.29(4), \chi^2/\text{d.o.f.} = 1.65/3$. These fits are plotted with dotted lines in the figure.

We note that the coarsening regime has been studied in previous work [33,34] using the growth of a length scale computed from the structure factor: $L(t) \propto t^{\alpha}$, $\alpha \approx 0.28$. If we reproduce the analysis of $L(t)$ in [34] with our data we obtain $\alpha = 0.26(2), \chi^2/\text{d.o.f.} = 1.82/3$ for $t D_r > 20$.

Finally, we compare the approach to the steady state to the dynamics of pressure fluctuations in the steady state by computing the time autocorrelation function of the instantaneous mean pressure, given by

$$C_p(t) = \frac{\langle p(s)p(s+t)\rangle - \langle p\rangle^2}{\langle p^2\rangle - \langle p\rangle^2}. \tag{8}$$

This function is shown in Fig. 7 for $\ell_p = 25$ and $\phi = 0.4$. The correlation function decays exponentially, allowing us to

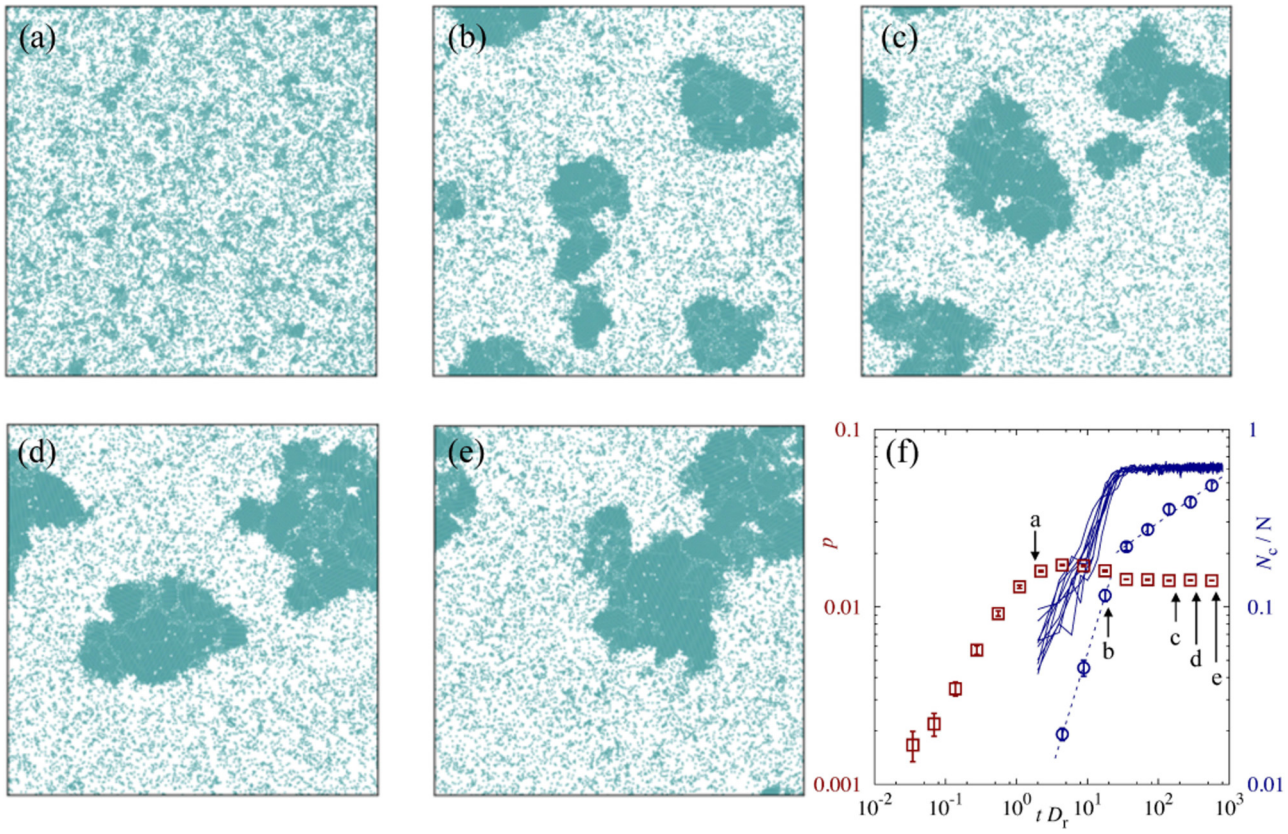

FIG. 6. Time evolution of pressure p (red squares), total cluster fraction N_c/N (blue lines), and largest cluster fraction N_1/N (blue circles) for a system with size $L = 400$, $\phi = 0.35$, and $\ell_p = 50$. N_c/N is shown in (f) for 10 individual runs to emphasize its robust steady state. Snapshots (a–e) show a single run, for times that correspond to the points in the (f), labeled respectively. The overshoot in pressure results from the onset of clustering, which dampens the swim and total pressure in the long-time limit. The steady state of pressure corresponds with the steady state of N_c, while N_1 continues to grow as the system coarsens.

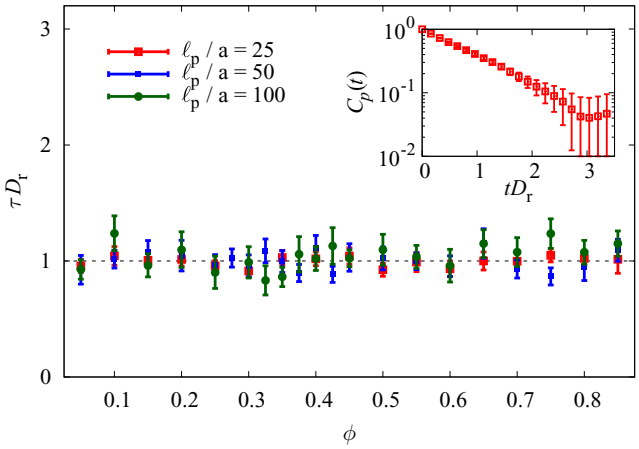

FIG. 7. Correlation time τ for $\ell_p = 25,50,100$ computed for the correlation function, Eq. (8). Inset shows an example of the steady-state correlation function, for $\phi = 0.4$ and $\ell_p = 25$. Even though the time needed to reach the steady state depends on ϕ (Fig. 5), once the steady-state has been reached τ is equal to the single-particle persistence time, $\tau = \tau_r = \ell_p/v_0$.

extract a relaxation time τ,

$$C_p(t) \simeq e^{-t/\tau}, \tag{9}$$

We find that τ does not depend on density and coincides with τ_r for all our runs (Fig. 7). Therefore, even though the time evolution of the pressure in the approach to the steady state is density dependent, once the steady state has been reached the only time scale for pressure fluctuations is given by the single-particle rotational diffusion.

V. CONCLUSIONS

We have examined the effects of finite system size and of the kinetics of MIPS on the pressure of ABPs in two dimensions. In a dilute gas of ABPs the finite-size effects on pressure for both open (periodic) and closed (particles in a square box) boundary conditions are quantitatively similar to what one would expect for a thermal gas. At finite density, finite-size effects are pronounced even for the periodic case. We find that the box size has to be several times larger than the persistence length of the particles to obtain results representative of bulk behavior. This has implications for studies in strip geometries [35], where a careful control is needed to avoid spurious anisotropies in the stresses.

For parameter values corresponding to MIPS, we have examined the correlation between the relaxation of the mean pressure to its steady-state value and the kinetics of clustering and phase separation. In this regime, the interplay between the decreasing swim pressure and the increasing direct pressure from interaction in the incipient clusters results in long, density-dependent time scales for approach to the steady state. The phase separation process shows two distinct dynamical regimes: a rapid growth corresponding to the formation of small clusters, followed by a slower regime of cluster coalescence and coarsening. These two regimes are reflected in the time evolution of the pressure that first grows rapidly during the small cluster nucleation when it is mainly controlled by the swim pressure of the gas, even overshooting its steady-state value, and then remains constant during coarsening when the net flux of particles between the dense and dilute phases vanishes. The overshoot of the swim pressure upon phase separation is a distinctive feature of active particles associated with crowding of the gas at the boundary of the dense phase. The cluster provides an effective bounding wall to the active gas, strongly suppressing the swim pressure. This effect has no analog in thermal systems where the kinetic contribution to the pressure is not affected by interactions nor by interfaces.

The total pressure has, however, been shown to remain equal across the two phases, confirming that this minimal model can be described in terms of an effective thermodynamics. The relationship between the kinetics of MIPS and the relaxation of pressure to its steady-state value additionally validates the use of equilibrium-like ideas as done in Ref. [32] to describe the coarsening kinetics.

ACKNOWLEDGMENTS

M.C.M. was supported by NSF-DMR-1305184 and NSF-DMR-1609208. M.C.M. and A.P. acknowledge support by the NSF IGERT program through award NSF-DGE-1068780. M.C.M., A.P., and D.Y. were additionally supported by the Soft Matter Program at Syracuse University. Our simulations were carried out on the Syracuse University HTC Campus Grid, which is supported by NSF award ACI-1341006, and on the Memento supercomputer. D.Y. acknowledges support by the MINECO (Spain) through Grant No. FIS2015-65078-C2-1-P as well as the resources, technical expertise, and assistance provided by BIFI-ZCAM (Universidad de Zaragoza).

[1] M. C. Marchetti, J. F. Joanny, S. Ramaswamy, T. B. Liverpool, J. Prost, M. Rao, and R. A. Simha, Rev. Mod. Phys. **85**, 1143 (2013).
[2] T. Vicsek, A. Czirók, E. Ben-Jacob, I. Cohen, and O. Shochet, Phys. Rev. Lett. **75**, 1226 (1995).
[3] J. Toner and Y. Tu, Phys. Rev. Lett. **75**, 4326 (1995).
[4] M. Ballerini, N. Cabibbo, R. Candelier, A. Cavagna, E. Cisbani, I. Giardina, V. Lecomte, A. Orlandi, G. Parisi, A. Procaccini, M. Viale, and V. Zdravkovic, Proc. Natl. Acad. Sci. USA **105**, 1232 (2008).
[5] B. Szabó, G. J. Szöllösi, B. Gönci, Z. Jurányi, D. Selmeczi, and T. Vicsek, Phys. Rev. E **74**, 061908 (2006).

[6] A. Saez, A. Buguin, P. Silberzan, and B. Ladoux, Biophys. J. **89**, L52 (2005).
[7] W. F. Paxton, K. C. Kistler, C. C. Olmeda, A. Sen, S. K. St. Angelo, Y. Cao, T. E. Mallouk, P. E. Lammert, and V. H. Crespi, J. Am. Chem. Soc. **126**, 13424 (2004).
[8] F. Ginot, I. Theurkauff, D. Levis, C. Ybert, L. Bocquet, L. Berthier, and C. Cottin-Bizonne, Phys. Rev. X **5**, 011004 (2015).
[9] J. Elgeti, R. G. Winkler, and G. Gompper, Rep. Prog. Phys. **78**, 056601 (2015).
[10] Y. Fily and M. C. Marchetti, Phys. Rev. Lett. **108**, 235702 (2012).
[11] J. Tailleur and M. E. Cates, Phys. Rev. Lett. **100**, 218103 (2008).
[12] Y. Fily, S. Henkes, and M. C. Marchetti, Soft Matter **10**, 2132 (2014).
[13] G. S. Redner, A. Baskaran, and M. F. Hagan, Phys. Rev. E **88**, 012305 (2013).
[14] M. E. Cates and J. Tailleur, Ann. Rev. Cond. Matt. Phys. **6**, 219 (2015).
[15] M. C. Marchetti, Y. Fily, S. Henkes, A. Patch, and D. Yllanes, Curr. Opin. Colloid Interface Sci. **21**, 34 (2016).
[16] J. Elgeti and G. Gompper, Europhys. Lett. **101**, 48003 (2013).
[17] X. Yang, M. L. Manning, and M. C. Marchetti, Soft Matter **10**, 6477 (2014).
[18] Y. Fily, A. Baskaran, and M. F. Hagan, Phys. Rev. E **91**, 012125 (2015).
[19] S. C. Takatori and J. F. Brady, Soft Matter, **10**, 9433 (2014).
[20] A. P. Solon, J. Stenhammar, R. Wittkowski, M. Kardar, Y. Kafri, M. E. Cates, and J. Tailleur, Phys. Rev. Lett. **114**, 198301 (2015).
[21] S. C. Takatori and J. F. Brady, Phys. Rev. E **91**, 032117 (2015).
[22] R. G. Winkler, A. Wysocki, and G. Gompper, Soft Matter **11**, 6680 (2015).
[23] A. C. Brańka and D. M. Heyes, Phys. Rev. E **60**, 2381 (1999).
[24] D. Amit and V. Martin-Mayor, *Field Theory, the Renormalization Group, and Critical Phenomena*, 3rd ed. (World Scientific, Singapore, 2005).
[25] S. A. Mallory, A. Šarić, C. Valeriani, and A. Cacciuto, Phys. Rev. E **89**, 052303 (2014).
[26] S. C. Takatori, W. Yan, and J. F. Brady, Phys. Rev. Lett. **113**, 028103 (2014).
[27] M. J. Louwerse and E. J. Baerends, Chem. Phys. Lett. **421**, 138 (2006).
[28] R. G. Winkler and C. C. Huang, J. Chem. Phys. **130**, 074907 (2009).
[29] B. M. Mognetti, A. Šarić, S. Angioletti-Uberti, A. Cacciuto, C. Valeriani, and D. Frenkel, Phys. Rev. Lett. **111**, 245702 (2013).
[30] At very high packing fraction, approaching or even surpassing the closed-packed limit, there are larger discrepancies, but we do not consider this regime here.
[31] A particle i is part of cluster $\mathcal{C}$ if it is interacting with any other disks in that cluster (i.e., if $r_{ij} \leqslant 2a$ for any $j \in \mathcal{C}$).
[32] G. S. Redner, C. G. Wagner, A. Baskaran, and M. F. Hagan, Phys. Rev. Lett. **117**, 148002 (2016).
[33] G. S. Redner, M. F. Hagan, and A. Baskaran, Phys. Rev. Lett. **110**, 055701 (2013).
[34] J. Stenhammar, A. Tiribocchi, R. J. Allen, D. Marenduzzo, and M. E. Cates, Phys. Rev. Lett. **111**, 145702 (2013).
[35] J. Bialké, J. T. Siebert, H. Löwen, and T. Speck, Phys. Rev. Lett. **115**, 098301 (2015).